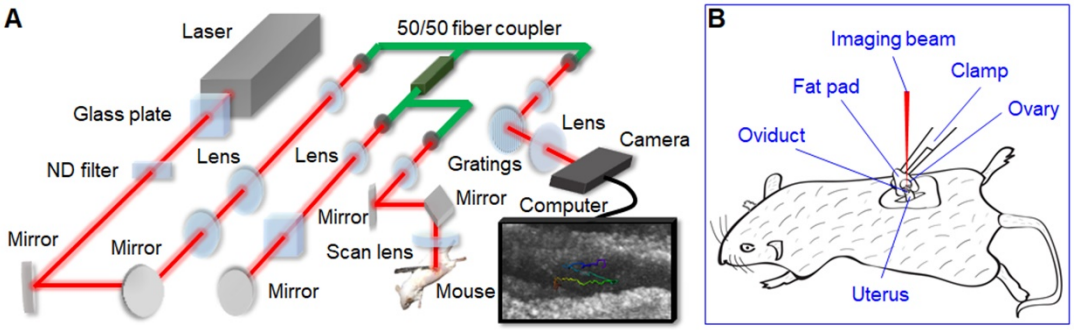

Fig. S1: *In vivo* OCT imaging setup for sperm tracking in the mouse oviduct. (A) Schematic of the spectral-domain OCT system used for live imaging, which provides an axial resolution of ~5 µm, a transverse resolution of ~4 µm, a 3D temporal resolution of 900 ms, and an imaging depth that covers the entire lumen of the mouse oviduct ampulla. (B) Illustration of the *in vivo* imaging approach where the reproductive organs of the anesthetized mouse are exposed for imaging; the fat pad associated with the ovary is stabilized using a surgical clamp.

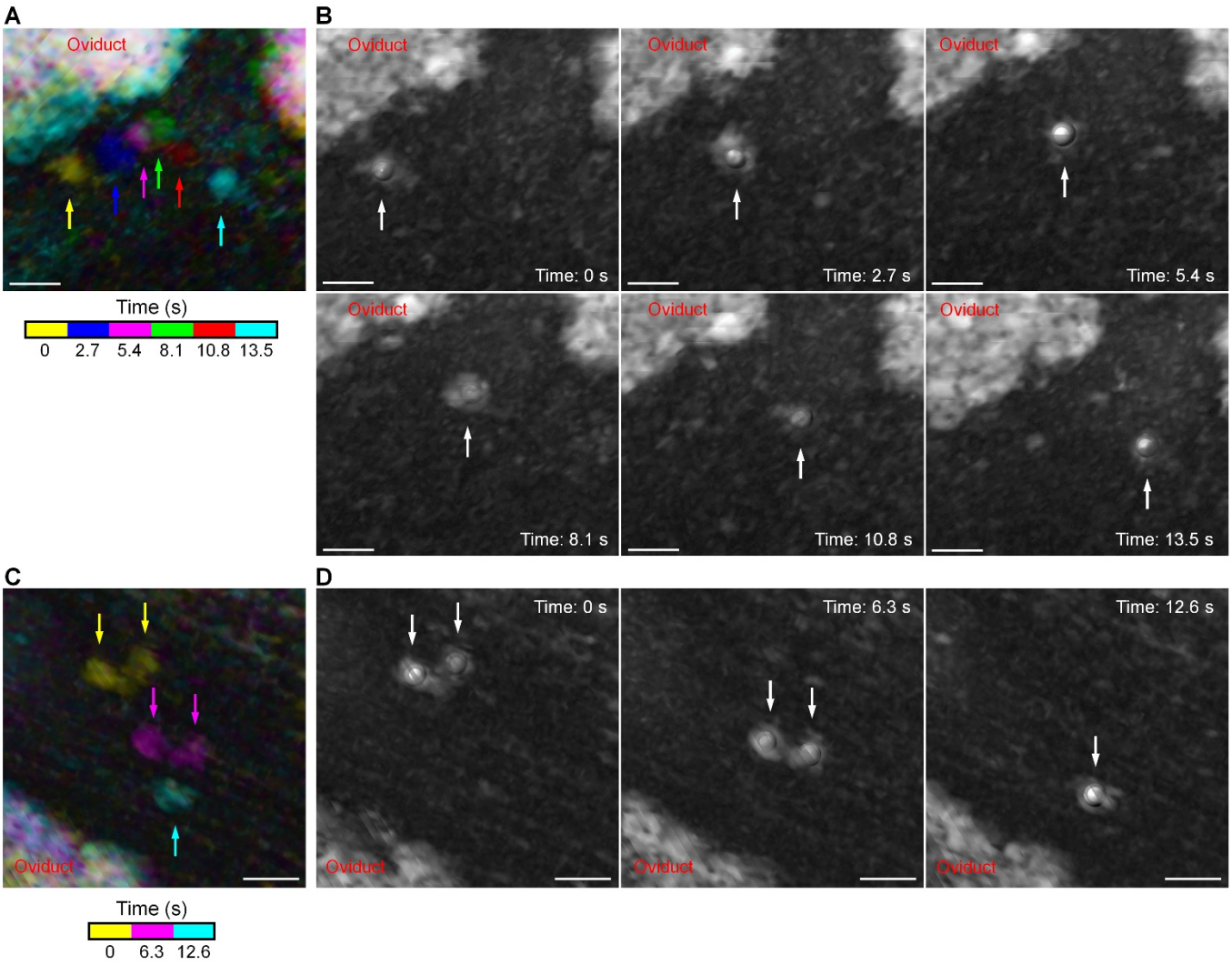

Fig. S2: Volumetric tracking of scatters in the oviduct with OCT. (A) An overlay of six images color-coded according to time. (B) Corresponding images at each time point. Balls indicate the position of the scatter used for tracking. (C) An overlay of color-coded images from three time points tracking the grouping of scatters. (D) Corresponding images with balls indicating the positions of the tracked scatters. The locations of the scatters over time are indicated with arrows. Overlay of all colors appears white, indicating non-moving structures. Scale bar are 30 µm.

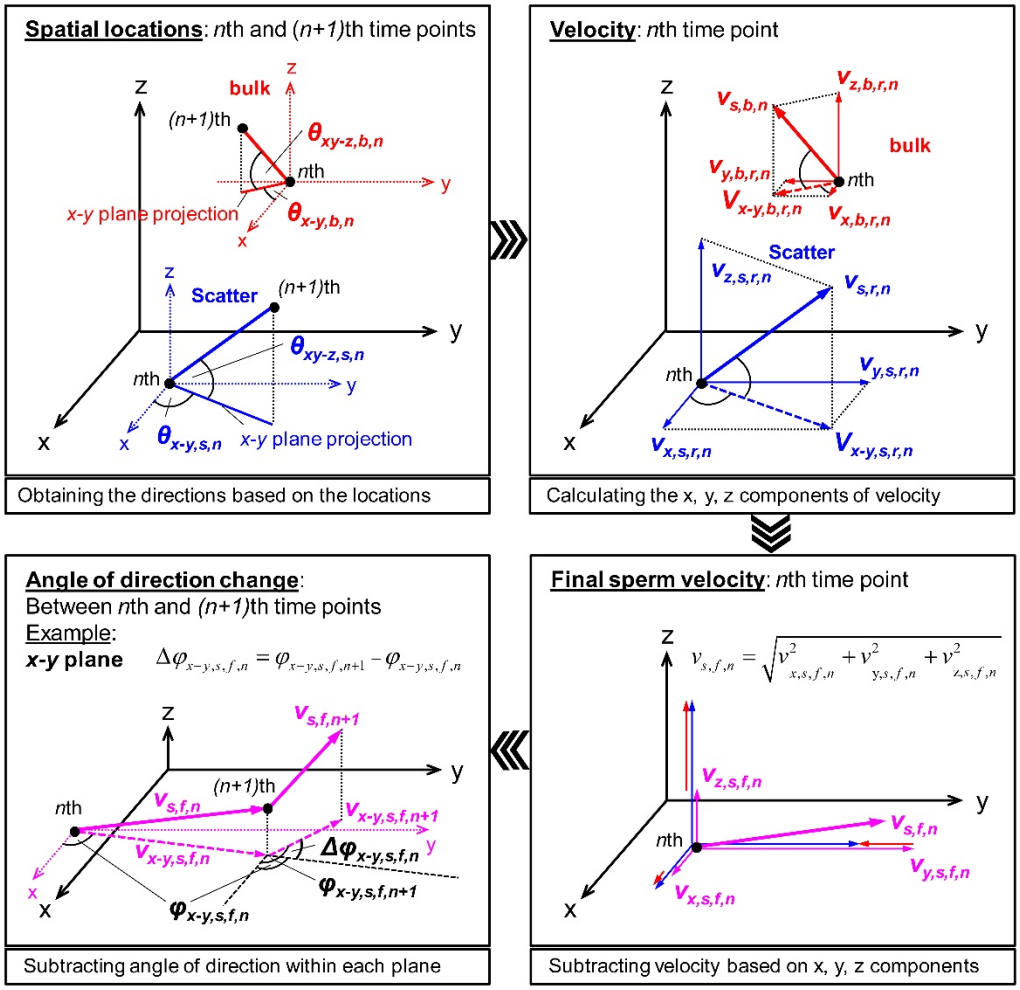

Fig. S3: Illustration of the oviduct bulk motion compensation. The bulk velocity and the scatter raw velocity are first determined based on the time series in 3D (1st step, up-left box). The velocity components along three axes are defined for both, the bulk and scatter movements (2nd step, up-right box). The compensation is achieved by subtracting the bulk velocity components from the scatter raw velocity components (3rd step, down-right). The angle of direction variation is calculated for each 2D projection between adjacent time points after bulk motion compensation (4th step, down-left).

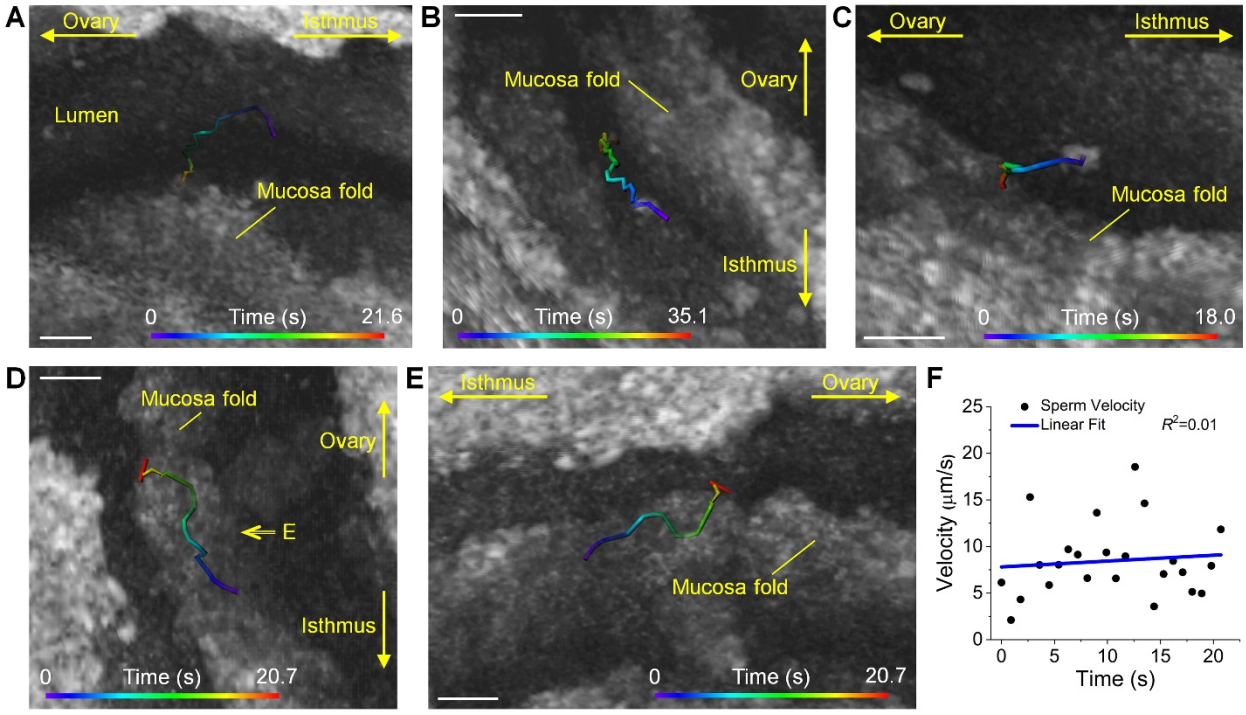

Fig. S4: Representative trajectories showing the sperm collection by the ampulla epithelium and the near-epithelium movement. (A-C) Three representative trajectories in the ampulla featuring sperm swimming toward the epithelium of the mucosa folds while traveling in the isthmus-to-ampulla direction. (D, E) Near-epithelial movement of the sperm swimming in the direction of isthmus-to-ampulla, visualized from two alternative angles, used for comparative analysis with the sperm collection process. (F) Corresponding plot of sperm velocity over time for the trajectory in (D, E). Scale bars are 50 μm.

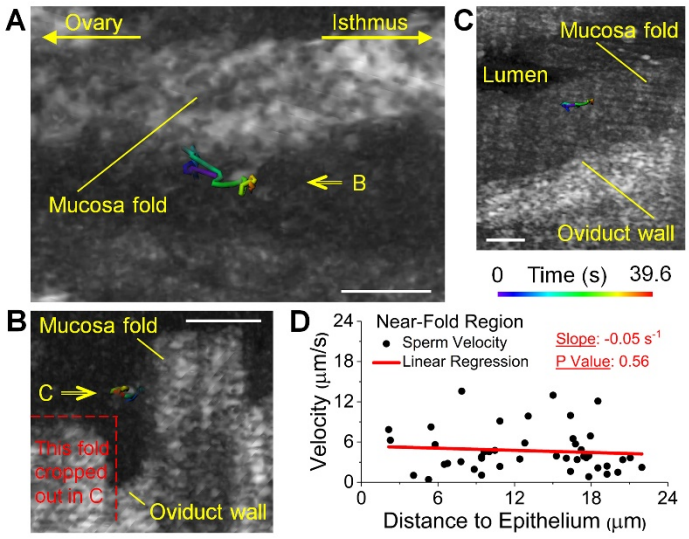

Fig. S5: A representative sperm trajectory in the near-fold region showing no dependence of the sperm velocity on the distance to the mucosa fold. (A-C) The representative sperm trajectory observed from three alternative angles. Arrows in (A) and (B) indicate the visualization angles for (B) and (C), respectively. The movement of sperm was close to the mucosa fold, but was relatively far from the oviduct wall, indicating the near-fold region. (D) Velocity of the sperm in (A-C) with respect to its distance to the mucosa fold indicates no influence from the distance on the velocity. N=44 for distance-velocity data, p=0.56, t statistics for the slope. Scale bars are 60 μm.

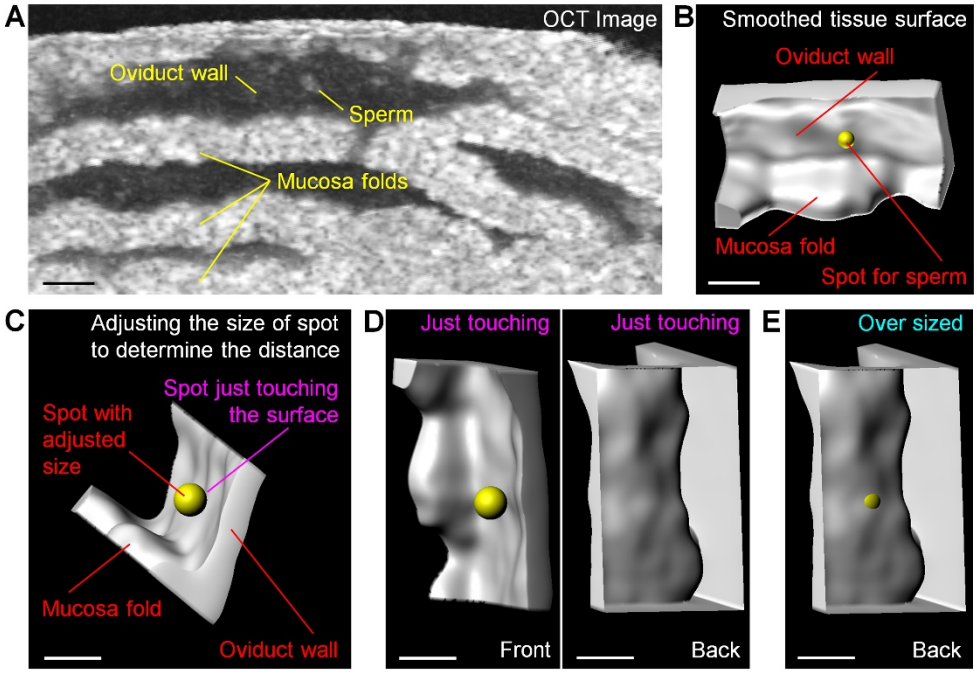

Fig. S6: Illustration for the measurement of distance between sperm and the ampulla epithelium in 3D. (A) A cross-sectional view of the OCT 3D reconstruction shows the oviduct wall, mucosa folds and sperm. (B) Surface rendering of the oviduct tissue with the spot representing the sperm location. (C) The size of the spot is adjusted to have it just touch the surface. (D) With the spot just touching the surface, representative visualizations are shown from the front and the back. (E) Over-sized spot can be clearly distinguished over the non-transparent isosurface from the back. The radius of the just-touching spot is taken as the distance to the oviduct epithelium. Scale bars are 50 µm.

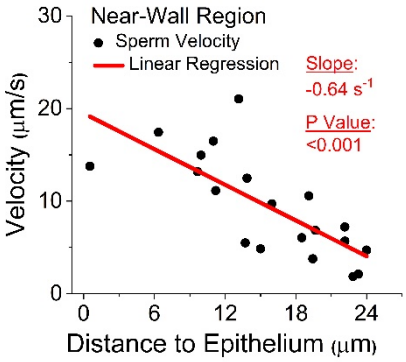

Fig. S7: Data from a representative sperm trajectory showing the dependence of the sperm velocity on the sperm-epithelium distance in the near-wall region of the oviduct ampulla. N=20 for distance-velocity data, $p=1.8\times10^{-4}$, t statistics for the slope.

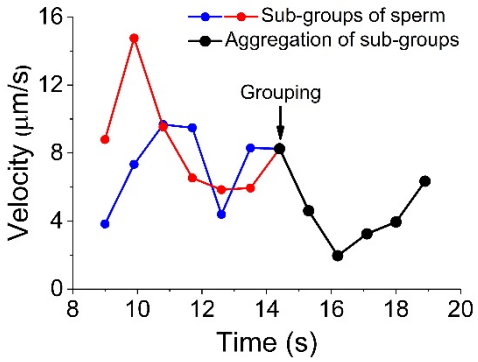

Fig. S8: Velocities of the sperm groups in Fig. 4C showing their response to grouping.

Movies

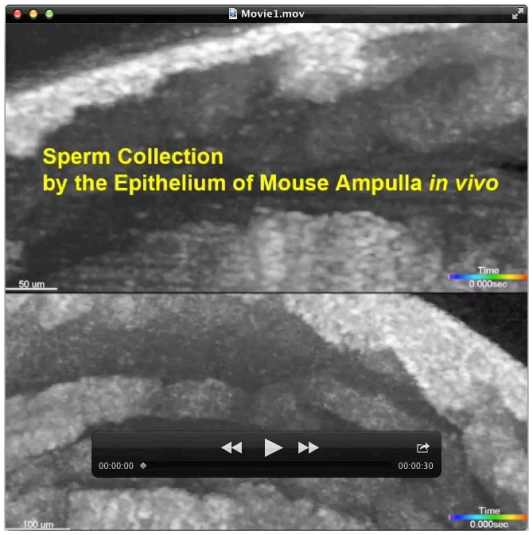

Movie 1: Sperm collection by the ampulla epithelium.

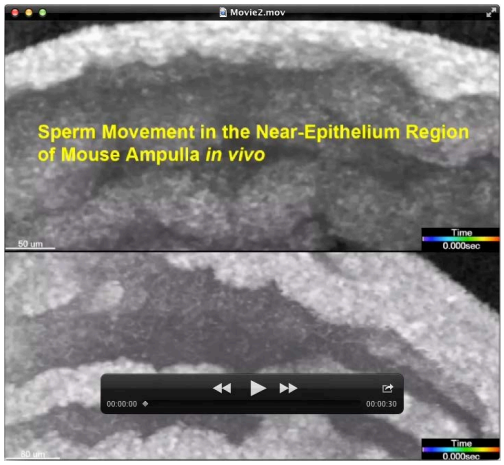

Movie 2: Near-epithelium movement of the sperm.

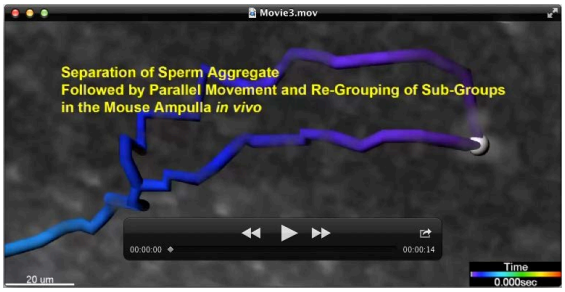

Movie 3: Separation of sperm aggregate followed by parallel movement and re-grouping of sub-groups.

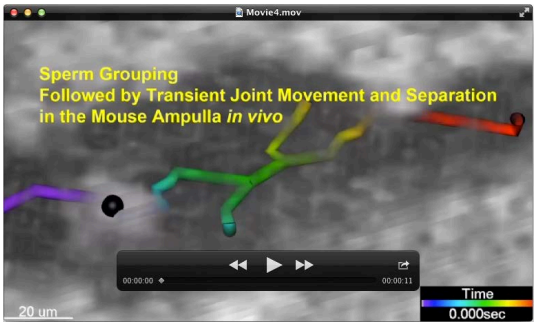

Movie 4: Sperm grouping followed by transient joint movement and separation.

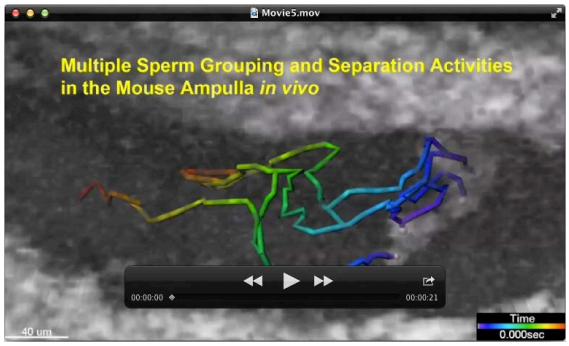

Movie 5: Multiple sperm grouping and separation activities.

Movie 6: Sperm swimming along adjacent mucosa folds.

Movie 7: Sperm swimming across the gap between adjacent mucosa folds.

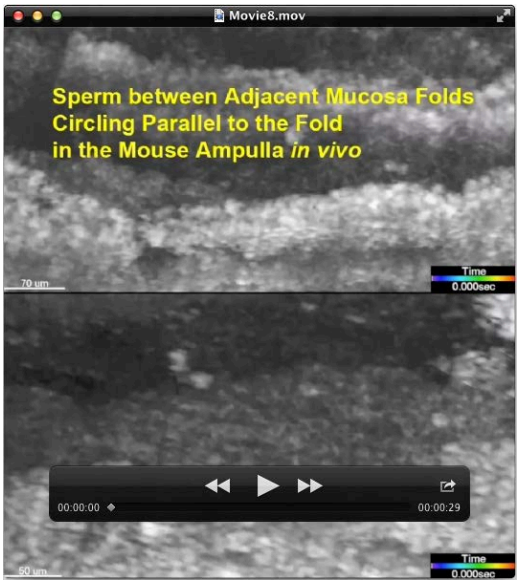

Movie 8: Sperm between adjacent mucosa folds circling parallel to the fold.

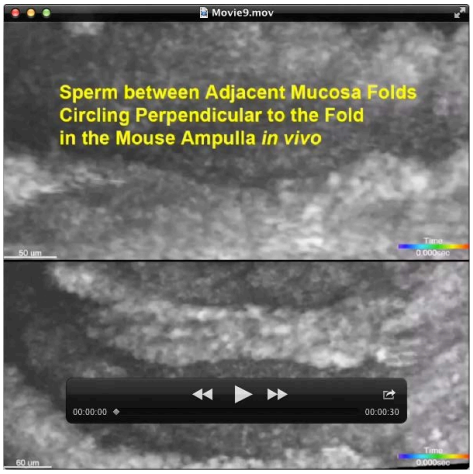

Movie 9: Sperm between adjacent mucosa folds circling perpendicular to the fold.